

Inferring chemical disequilibrium biosignatures for Proterozoic Earth-like exoplanets

Received: 1 December 2022

Accepted: 26 October 2023

Published online: 22 January 2024

 Check for updates

Amber V. Young ¹✉, Tyler D. Robinson ², Joshua Krissansen-Totton³, Edward W. Schwieterman ⁴, Nicholas F. Wogan⁵, Michael J. Way ^{6,7}, Linda E. Sohl ^{6,8}, Giada N. Arney ⁹, Christopher T. Reinhard ¹⁰, Michael R. Line ¹¹, David C. Catling ^{3,12} & James D. Windsor ¹

Chemical disequilibrium quantified using the available free energy has previously been proposed as a potential biosignature. However, researchers remotely sensing exoplanet biosignatures have not yet investigated how observational uncertainties impact the ability to infer a life-generated available free energy. We pair an atmospheric retrieval tool to a thermodynamics model to assess the detectability of chemical disequilibrium signatures of Earth-like exoplanets, focusing on the Proterozoic eon when the atmospheric abundances of oxygen–methane disequilibrium pairs may have been relatively high. Retrieval model studies applied across a range of gas abundances revealed that order-of-magnitude constraints on the disequilibrium energy are achieved with simulated reflected-light observations for the high-abundance scenario and high signal-to-noise ratios (50), whereas weak constraints are found for moderate signal-to-noise ratios (20–30) and medium- to low-abundance cases. Furthermore, the disequilibrium-energy constraints are improved by using the modest thermal information encoded in water vapour opacities at optical and near-infrared wavelengths. These results highlight how remotely detecting chemical disequilibrium biosignatures can be a useful and metabolism-agnostic approach to biosignature detection.

Exoplanet exploration science is making rapid progress towards the detection and characterization of potentially habitable worlds¹. Continuing^{2,3} and near-future exoplanet strategies⁴ will focus on the search for atmospheric gases, including the chemical signatures of life (or biosignatures)^{5–7}. Recently, the Decadal Survey on Astronomy and

Astrophysics 2020 report⁴ recommended space-based high-contrast imaging of potentially life-bearing exoplanets as a leading priority for the coming decade. When attempting to infer whether a distant world is inhabited, the chemical disequilibrium is a potential indicator of life and has a long history of study in Solar System planetary environments^{8–10}.

¹Department of Astronomy and Planetary Sciences, Northern Arizona University, Flagstaff, AZ, USA. ²Lunar and Planetary Laboratory, University of Arizona, Tucson, AZ, USA. ³Earth and Space Sciences, University of Washington, Seattle, WA, USA. ⁴Department of Earth and Planetary Sciences, University of California Riverside, Riverside, CA, USA. ⁵Space Science Division, NASA Ames Research Center, Moffett Field, CA, USA. ⁶NASA Goddard Institute for Space Studies, New York, NY, USA. ⁷Theoretical Astrophysics Department of Physics and Astronomy, Uppsala University, Uppsala, Sweden. ⁸Center for Climate Systems Research, Columbia University, New York, NY, USA. ⁹NASA Goddard Space Flight Center, Greenbelt, MD, USA. ¹⁰Earth and Atmospheric Sciences, Georgia Tech, Atlanta, GA, USA. ¹¹School of Earth and Space Exploration, Arizona State University, Tempe, AZ, USA. ¹²Astrobiology Program, University of Washington, Seattle, WA, USA. ✉e-mail: Amber_Young86@nau.edu

A key example is the coexistence of O₂ and CH₄ in Earth's atmosphere because the strong biological production rates of CH₄ are able to maintain this gas at appreciable levels despite its relatively short chemical lifetime (roughly a decade) in an oxidizing atmosphere.

A primary metric for quantifying chemical disequilibrium involves calculating the difference in chemical energy associated with an observed system and that system's theoretical equilibrium state. Recent work has explored the application of one such metric—the available Gibbs free energy—to Solar System worlds and to Earth's planetary evolution^{11–13}. Although the available Gibbs free energy is a promising metric for interpreting chemical disequilibrium biosignatures, little is known about how observational uncertainties will impact our ability to constrain the available Gibbs free energy for Earth-like exoplanets, where 'Earth-like' refers to an ocean-bearing, Earth-sized world with surface pressures and temperatures like those on Earth and with an atmosphere dominated by N₂, H₂O and CO₂ with trace amounts of CH₄ and varying levels of O₂.

Exoplanet atmospheric characterization, including the search for biosignature gases, proceeds through retrieval analysis or atmospheric inference (for example, refs. 14–18). In short, a retrieval framework enables the statistical exploration of atmospheric states that are consistent with a given set of spectral observations, whether these are real or simulated. Although retrieval models do not directly constrain quantities like the available Gibbs free energy, pairing an exoplanet atmospheric retrieval model with a thermochemical tool—as detailed in Methods—enables inferences of both atmospheric chemical abundances and the associated disequilibrium state of the atmosphere. As described in Methods, simulated reflected-light observations of an Earth-like planet are created with uncertainties specified by the V-band (0.55 μm) signal-to-noise ratio (SNR). Applying inverse modelling techniques to these simulated observations for several randomized observational noise realizations then maps the observational quality to the expected constraints on the available Gibbs free energy.

The analyses presented here focus on directly imaged Proterozoic Earth analogues with reflectance spectral data spanning near-infrared, optical and ultraviolet wavelengths at resolving powers of 70, 140 and 7 (motivated by Decadal Survey mission concept reports^{19,20}). This eon represents roughly half of Earth's history and is notable for its oxygenated atmosphere, which may have had enhanced atmospheric methane concentrations (compared to modern Earth), thereby presenting an ideal time period for detecting an O₂–CH₄ disequilibrium. The retrieval studies described in this paper explore a range of concentrations for key gases in Proterozoic Earth's atmosphere and were adopted from a span of Earth evolutionary scenarios summarized in a review²¹. Our high- and low-concentration scenarios are identical to mid-Proterozoic extremes from this review, and an intermediate-concentration case was generated by computing the logarithmic geometric mean of the high and low cases.

Figure 1 shows modelled constraints on the atmospheric available Gibbs free energy (in joules per mole of atmosphere) that would be expected from observations of Proterozoic Earth analogues in reflected light. Each result is broken up into three atmospheric composition categories of high, medium and low biosignature gas abundances. The simulated observations were conducted at several SNRs for each abundance category. Most of these reflected-light cases present available Gibbs free energy posteriors that are consistently peaked at lower Gibbs free energy values but with statistically significant tails to higher values. In our simulations, the log available Gibbs free energy is found to be no larger than 1.30, 1.13 or 1.21 J mol⁻¹ at 95% confidence (inferred from the marginal cumulative distributions) for SNR = 20, 30 or 50 for the medium-abundance case and 0.47, 0.68 or 0.03 J mol⁻¹ for the low-abundance case. By contrast, the uncertainty on the available Gibbs free energy for the high-abundance case goes down to as low as an order of magnitude for the SNR = 50 observational case (Table 1). In the high-abundance scenario (Fig. 1a), the distributions of the posteriors

derived from the simulated SNR = 20 or 30 observations have a dual peak. Given the randomization of the simulated observational data points, retrievals at these SNRs could occasionally constrain the O₂ abundance. Thus, one peak corresponds to cases in which O₂ is well detected and the other peak corresponds to non-detections.

The constraints on the available Gibbs free energy are most strongly dependent on the quality of the inferences for the O₂ abundance, CH₄ abundance and atmospheric temperature, as shown in Fig. 2. This is consistent with thermodynamic theory, which has shown that the Gibbs free energy is strongly dependent on temperature and only weakly dependent on pressure²². In the high-abundance case with SNR = 20, the results show a large uncertainty on the inferred O₂ abundance. This introduced a substantial uncertainty on the available Gibbs free energy for this particular case. However, higher observational SNRs of 30 and 50 at high abundance showed better constraints on O₂, which led to improved constraints on the available Gibbs free energy. These trends also held true for the CH₄ posteriors in the high-abundance case. The retrieval analyses for the medium and low cases largely resulted in broad upper limit constraints for O₂ and CH₄ at each of the observational SNR scenarios tested here. Reasonable atmospheric temperature constraints were seen for all abundance cases and observing scenarios, which stemmed from adequate constraints on the shape of the atmospheric water vapour bands across the spectral range for all modelled scenarios. Table 1 details the 16th, 50th and 84th percentile values for the marginal O₂, CH₄ and temperature distributions (corresponding to the 1σ values for a Gaussian distribution).

Most fundamentally, the results for the high-abundance scenario demonstrate that strong detections of O₂ and CH₄ absorption features lead to tight constraints on the resulting available Gibbs free energy, thereby enabling an inference of the extent of chemical disequilibrium in the atmosphere of an Earth-like exoplanet. Figure 3 highlights spectral features of several species (O₂, CH₄, O₃, CO₂ and H₂O) across the range of modelled Proterozoic Earth scenarios. In the near-infrared, optical and ultraviolet spectral range explored in this work, the strongest O₂ feature is the oxygen A-band at 0.762 μm. There are several CH₄ features within the 1.6–1.8 μm wavelength range, indicated in orange. Each colour-coded absorption feature for O₃, CO₂, CH₄ and O₂ is accentuated by a factor of 2 relative to the original input abundance to highlight the precision needed to observe each species.

Constraining the available Gibbs free energy is a promising characterization strategy that synergizes well with established techniques for biosignature gas detection. In practice, it is possible to infer an upper limit on the available Gibbs free energy and, for more optimistic cases, proper constraints can be obtained on the free energy for Proterozoic Earth-like planets. For high-abundance cases, in particular, it is possible to place constraints on the available Gibbs free energy to within an order of magnitude with SNR = 50 observations. This could be feasible with a future direct-imaging mission for exoplanets, but future work is necessary to understand any systematic barriers to achieving this level of SNR. Also note that the detection of the O₂–CH₄ disequilibrium is highly sensitive to the near-infrared spectral features that drive the quality of the CH₄ abundance constraints and is also, in part, enabled by atmospheric temperature constraints from thermal effects in molecular band shapes (especially in the near-infrared). Such spectral features may not be observable for all targets as the inner working angle for high-contrast imaging systems, especially coronagraphs, expands linearly with wavelength, thus further indicating the importance of a small inner working angle for a future mission. Features shortward of 1.8 μm observed with a 6 m telescope would be accessible for targets within ~8 pc. For a 6 m-class space telescope with noise properties modelled on the LUVOIR-B concept^{20,23}, the high-SNR cases explored here could be achieved for an Earth-like target around a solar host at distances of 5–7 pc with an investment of 2–4 weeks of observing time (in line, for example, with planned expenditures for high-value targets in the Habitable Exoplanet Observatory concept study¹⁹). According to a recently

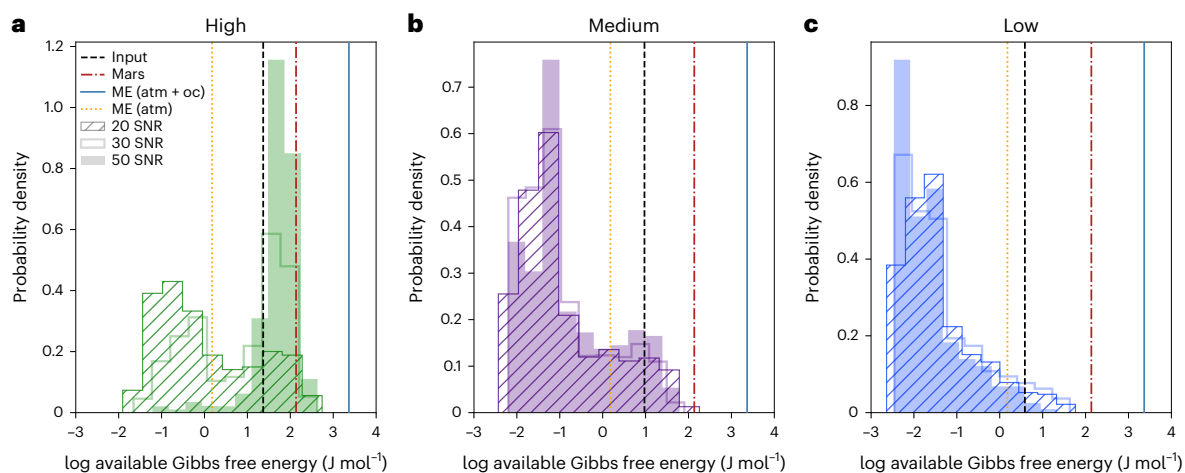


Fig. 1 | Available Gibbs free energy posterior distributions inferred from simulated reflected-light observations for different Proterozoic Earth models. a, Marginal posterior distribution of the log of the available Gibbs free energy for the high-abundance case, derived from SNR = 20 (hatched), 30 (unfilled) and 50 (solid fill) simulated reflected-light observations. Vertical black (dashed), orange (dotted), red (dot-dashed) and blue (solid) lines in all

three panels represent the input value and previously reported values for the available Gibbs free energy of modern Earth (atmosphere only case), Mars and modern Earth (atmosphere and ocean case), respectively¹¹. **b**, Same as **a** but for the medium-abundance case. **c**, Same as **a** but for the low-abundance case. atm, atmosphere only case; atm + oc, atmosphere and ocean case; ME, modern Earth.

Table 1 | Summary of the parameters, input values and 1 σ confidence intervals (taken from the 16th, 50th and 84th percentile values) for the high, medium and low atmospheric abundance scenarios that were modelled

Parameter	Abundance	Input	SNR=20	SNR=30	SNR=50
log O ₂	High	-2.01	-2.92 ^{+1.45} _{-4.76}	-2.07 ^{+0.49} _{-4.54}	-1.66 ^{+0.24} _{-0.23}
	Medium	-3.01	-6.08 ^{+2.65} _{-2.67}	-6.02 ^{+2.68} _{-2.71}	-6.29 ^{+2.54} _{-2.52}
	Low	-4.01	-6.60 ^{+2.37} _{-2.31}	-6.73 ^{+2.25} _{-2.23}	-7.00 ^{+2.05} _{-2.05}
log CH ₄	High	-4.54	-4.36 ^{+0.62} _{-3.04}	-4.20 ^{+0.35} _{-1.28}	-4.11 ^{+0.27} _{-0.32}
	Medium	-4.94	-6.07 ^{+1.52} _{-2.66}	-6.29 ^{+1.57} _{-2.52}	-5.31 ^{+0.71} _{-2.94}
	Low	-5.53	-7.19 ^{+1.92} _{-1.90}	-6.87 ^{+1.92} _{-2.12}	-7.44 ^{+1.76} _{-1.75}
log CO ₂	High	-1.16	-0.65 ^{+0.36} _{-0.39}	-0.79 ^{+0.24} _{-0.26}	-0.75 ^{+0.22} _{-0.20}
	Medium	-2.23	-2.28 ^{+0.48} _{-3.27}	-2.14 ^{+0.27} _{-0.34}	-2.19 ^{+0.22} _{-0.27}
	Low	-3.31	-6.36 ^{+2.54} _{-2.48}	-6.40 ^{+2.44} _{-2.46}	-6.75 ^{+2.25} _{-2.21}
T _o (K)	High	288	259.91 ^{+32.18} _{-26.39}	272.23 ^{+21.41} _{-20.62}	266.86 ^{+12.44} _{-12.24}
	Medium	288	267.84 ^{+30.15} _{-27.70}	273.84 ^{+22.47} _{-28.01}	266.13 ^{+14.21} _{-12.44}
	Low	288	255.31 ^{+25.06} _{-19.79}	258.34 ^{+23.07} _{-17.31}	263.09 ^{+15.18} _{-13.10}
log available Gibbs free energy (log J mol ⁻¹)	High	1.3687	0.17 ^{+1.69} _{-0.95}	1.28 ^{+0.59} _{-1.72}	1.76 ^{+0.28} _{-0.32}
	Medium	0.9739	-1.24 ^{+1.59} _{-0.65}	-1.23 ^{+1.54} _{-0.60}	-1.16 ^{+1.74} _{-0.62}
	Low	0.5853	-1.65 ^{+1.11} _{-0.55}	-1.63 ^{+1.18} _{-0.60}	-1.74 ^{+0.81} _{-0.57}

proposed target star list for the Habitable Worlds Observatory²⁴, about 26 stars are within that 7 pc limit. Two important observation-related caveats are that the retrievals assume that the planetary orbit is well constrained at that planet-to-star flux ratio and that the retrievals could be treated as being independent of time over the course of an observation. As an observing strategy, performing a baseline analysis at lower SNRs may help us identify potentially exciting targets for more detailed follow-up observations and provide upper limit constraints on potential chemical disequilibrium signals for a subset of targets.

From an observational perspective, characterizing the CH₄ and O₂ abundances are essential to inferring the atmospheric chemical disequilibrium signal of Earth analogues over most of their evolutionary history. Although the results presented here are focused on the

detectability of O₂ and CH₄ from space with reflected-light observations in visible and near-infrared wavelengths, similarly effective observations could be done from the ground and in other spectral ranges. For example, extremely large telescopes could attempt O₂ detections for Earth-like planets orbiting nearby M dwarfs^{25–28}. Ground-based observations would complement continuing efforts with the James Webb Space Telescope (JWST), as constraining Earth-like abundances of O₂ is a known challenge²⁹. Analogous transit scenarios relevant to the JWST NIRSpec instrument are explored in the Supplementary Information (Supplementary Figs. 1 and 2), which shows that the available Gibbs free energy is difficult to constrain (most probably due to non-detections of O₂ from the simulated observations). Conversely, molecular oxygen may be detectable in the mid-infrared with transit spectroscopy by

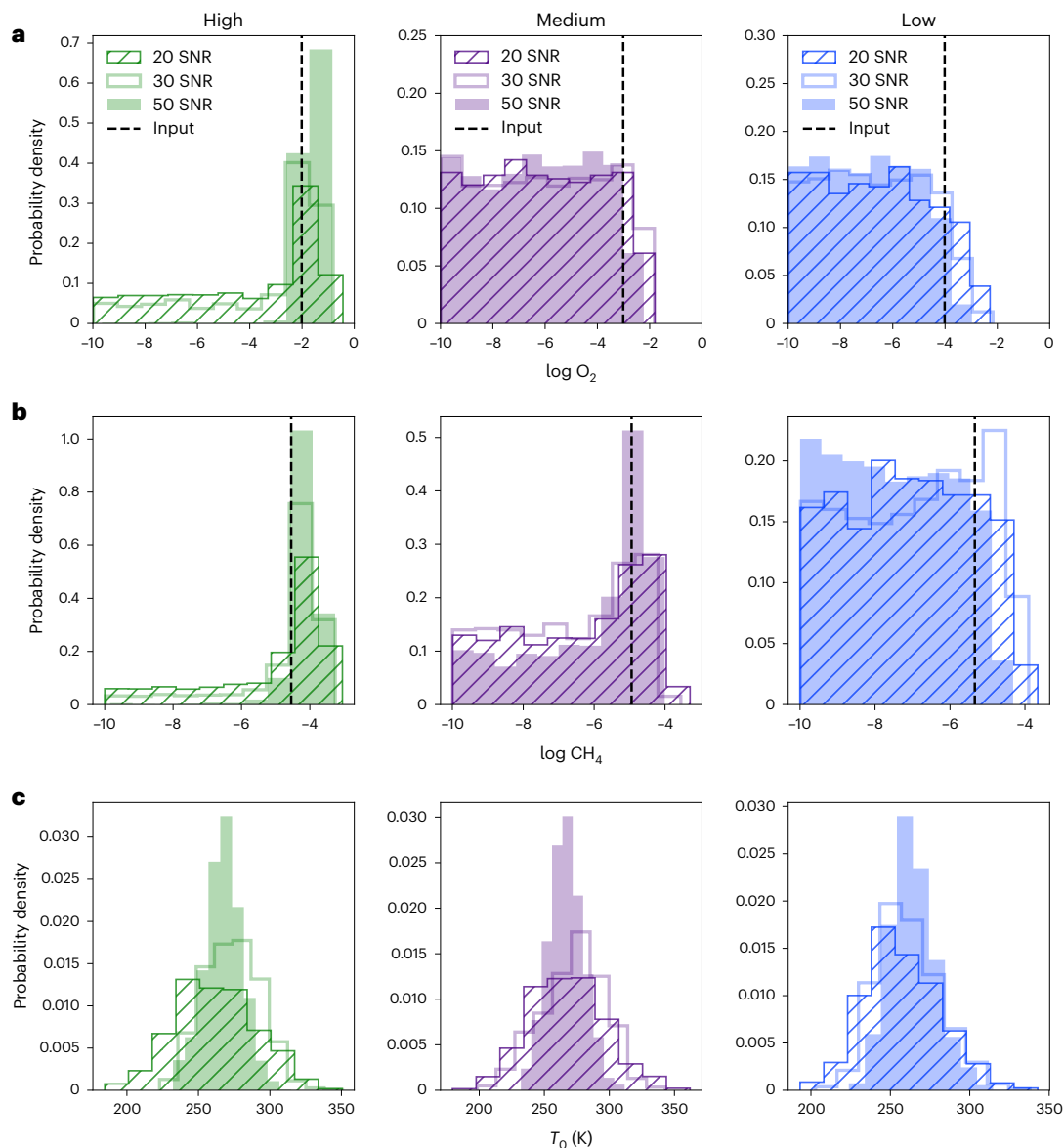


Fig. 2 | Posterior distributions for key retrieved atmospheric parameters for different noise levels and Proterozoic Earth models. a, The marginal posterior probability distributions for the retrieved log abundance of O_2 in the high (green), medium (purple) and low (blue) abundance cases. Each distribution is inferred from simulated reflected-light observations at SNR = 20 (hatched),

30 (unfilled) and 50 (solid fill). The vertical black dashed lines represent the input value for each parameter (the input is calculated using column-integrated volume mixing-ratio profiles for each gas phase species). **b**, Same as **a** but for the methane constraints. **c**, Same as **a** but for the atmospheric temperature constraints.

observing O_2 collision-induced absorption features near $6.4 \mu\text{m}$ with the JWST MIRI instrument³⁰. Although O_2 does not produce strong features in the emission spectrum of an Earth-like exoplanet, if O_2 abundances could be inferred from O_3 abundances³¹ then detections of O_3 in the mid-infrared at $9.7 \mu\text{m}$ with low- or moderate-resolution spectroscopy could provide the requisite constraints on O_2 . The LIFE (Large Interferometer for Exoplanets) mission concept, for example, could constrain O_3 abundances at SNRs >10 in the mid-infrared³². Ozone also has absorption features in the ultraviolet (for example, the Hartley–Huggins band at $0.25 \mu\text{m}$ and the subtler Chappuis bands from 0.5 to $0.7 \mu\text{m}$), which could be detectable with the Habitable Worlds Observatory using low- or moderate-resolution reflected-light observations as well (Supplementary Fig. 3c). CH_4 has key absorption bands throughout the optical, near-infrared and mid-infrared, so could be detected by reflectance, transmission or emission spectroscopy and would require resolving powers of roughly 30–40, depending on abundance (for example, refs. 28,29,33–35).

The Proterozoic eon is a potentially ideal Earth-like context for constraining the atmospheric O_2 – CH_4 chemical disequilibrium gas pair for an Earth-like planet around a G-type star due to a probably higher abundance of CH_4 , a rise in O_2 relative to the Archean Earth, and the longevity of this signal over a 2 Gyr period. An Archean Earth-like atmosphere may have a modest atmospheric chemical disequilibrium signature driven by the CH_4 – CO_2 gas pair¹². However, abiotic sources for CH_4 production would need to be explored¹². Modern Earth has substantially less atmospheric CH_4 , making detection of the O_2 – CH_4 atmospheric signature challenging, although the photochemistry for a modern Earth-like planet around an M or K dwarf may generate substantially more CH_4 in atmospheres with modern levels of O_2 (for example, refs. 36,37). Thus, the concept of remotely detectable disequilibrium-energy biosignatures could apply to Earth-like worlds around a very wide range of stellar host types. For any exoplanet, the stellar photochemical context will be vital to consider when evaluating potential biosignatures. Nevertheless, our results offer a window

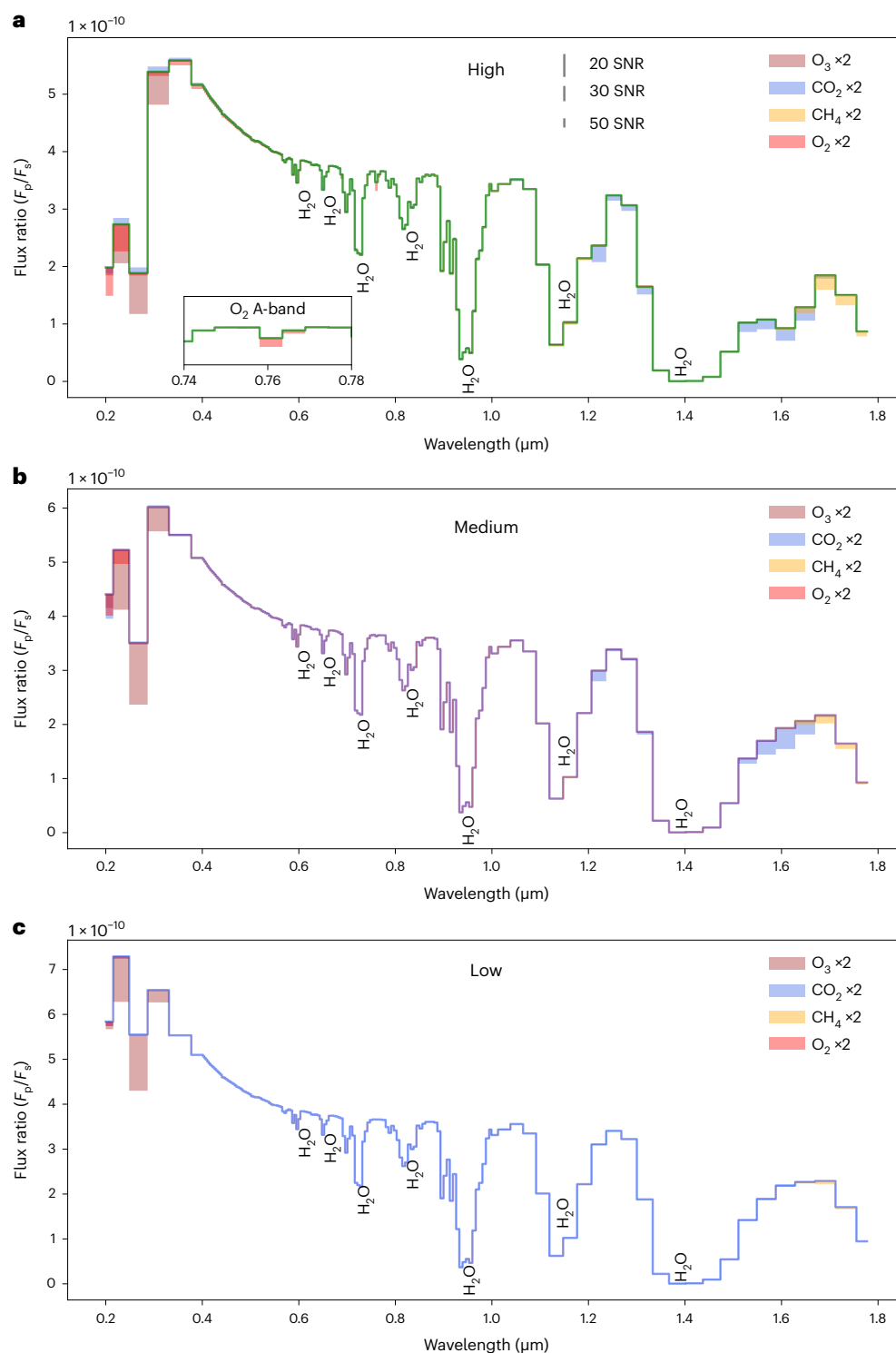


Fig. 3 | Simulated reflected-light spectra for Proterozoic Earth cases.

a–c. The x axes indicate the wavelength in micrometres and the y axes represent the planet-to-star flux ratio. **a.** Simulated reflected-light spectrum for the high-abundance case (green). Absorption features for O₃ (brown), CO₂ (blue), CH₄ (yellow) and O₂ (red) are shown and their input abundances are multiplied by a factor of 2. Water vapour absorption features are labelled with text. The legend

for the grey error bars shows the scaling for each noise instance (SNR = 20, 30 or 50). The inset highlights the O₂ A-band feature at 0.76 μm. **b.** Simulated reflected-light spectrum for the medium-abundance case (purple). Each input abundance is multiplied by a factor of 2 to show its effect. **c.** Simulated reflected-light spectrum for the low-abundance case (blue). The denoted species absorption features are shown and their input abundances are multiplied by a factor of 2.

into the characterization of an Earth–Sun twin as an analogue for similar exoplanets.

The thermodynamic systems modelled here represent only the chemical disequilibrium in the atmosphere. Oceans can provide an

additional source of chemical disequilibrium and, in fact, the maintenance of N₂ and O₂ in the presence of liquid water (for Proterozoic and modern Earth) and the maintenance of CO₂, N₂ and CH₄ in the presence of liquid water (for Archean Earth) are major contributors to

disequilibrium energy over time¹². There is the potential for remotely detecting exoplanetary oceans with reflected light^{38–41}. However, inferring the available energy requires constraints on the planet's ocean volume, which may be quite challenging to constrain remotely. Thus, atmospheric disequilibrium constraints are probably conservative, at least for ocean-bearing worlds. In general, the inability to easily constrain ocean volume (or its chemical state) or the inability of retrieval to fully detect all gaseous species means that the constraints on the atmospheric available Gibbs free energy are probably conservative.

Discriminating false positives, for which an abiotically driven signal could mimic a true biosignature, is especially crucial for interpreting chemical disequilibrium signatures, as false positives for O₂ have been heavily studied^{42–46}. The holistic interpretation of a given chemical disequilibrium signal will require not only a quantification of the extent of the signal but also an inference of the chemical species driving the signature and their production and loss mechanisms⁶. A previous study by Wogan and Catling¹³ outlined the potential abiotic mechanisms that generate free energy and even cases where a lack of free energy could lead to a false negative scenario.

A known environment with an excess amount of abiotically produced free energy is Mars. In fact, estimates of chemical disequilibrium for the Proterozoic Earth are lower than those for modern Mars (24 J mol⁻¹ versus 136 J mol⁻¹, respectively). However, the available Gibbs free energy produced on Mars is driven by the O₂–CO gas pair (abiotically generated by CO₂ photolysis), whereas abiotic sources for free energy in the Proterozoic Earth atmosphere are negligible (Supplementary Fig. 4). The direct-imaging characterization of a true Mars analogue exoplanet would be challenging due to the tenuous nature of the atmosphere, a larger orbital distance than Earth-like targets and the overall smaller size. However, Mars-like worlds with substantial available Gibbs free energy due to photochemistry may represent an important category of false positives. Mars has very cold, dry atmospheric conditions with a majority of its atmosphere comprising CO₂, which can be readily photolysed. Given this context, one would need to constrain the photochemical environment of a Mars analogue to distinguish it from a Proterozoic Earth-like case. This would require that atmospheric constraints (for example, species abundances, planetary surface pressure and atmospheric temperature) are obtained alongside a characterization of the host stellar spectrum (especially at ultraviolet wavelengths). It is especially important to characterize the abundances of CO₂, CO and abiotic O₂. CO₂ and CO have absorption features in the near-infrared around 1.6 μm and CO₂ has additional, weaker features at shorter near-infrared wavelengths. CO absorption in this wavelength range is particularly weak and would probably require high CO partial pressures to be detectable, thus implying that it might be difficult to detect the abiotic disequilibrium energy for such worlds.

In any given search, a planet's retrieved chemical disequilibrium must be considered alongside other contextual information when establishing the biogenicity. For example, a disequilibrium that requires gas fluxes incompatible with abiotic explanations is more probably due to life. Additionally, planets with 'edible' disequilibria (that is, easily surmountable kinetic barriers) that might be expected to be readily consumed as a metabolic fuel by a resident biosphere may serve as 'anti-biosignatures'¹³. In general, detecting atmospheric chemical disequilibrium would require that the associated chemical species are mixed well in the atmosphere whereas more localized, non-global signatures would be much more difficult to constrain.

In summary, searching for chemical disequilibrium biosignatures will be a promising endeavour for exoplanet characterization efforts, and future missions should consider this approach when developing their observational strategies. For Earth-like analogues, access to O₂ and CH₄ spectral features is key and will hinge on sufficient resolving power and broad spectral coverage to retrieve relevant gas features. Maximizing the potential to place tight constraints on these chemical species will probably require high-SNR observations at wavelengths

spanning into the near-infrared, implying that this technique may be most relevant for the best exoplanetary candidates. Alongside understanding planets and stars as systems⁶, chemical disequilibrium biosignatures will be a powerful tool for future observations.

Methods

This study incorporated an exoplanet atmospheric retrieval model that was coupled to a thermodynamics Gibbs free energy tool to explore how observational quality influences our ability to interpret and quantify chemical disequilibrium signals from simulated reflected-light observations. The photochemical model Atmos was used to explore a range of atmospheric compositions spanning high, medium and low biosignature gas abundances, and these were then used to generate simulated spectra according to each abundance case. Thereafter a spectral retrieval model, rfast, was used to map out the posterior distributions of relevant atmospheric and planetary parameters consistent with a given simulated observation. The rfast and the Gibbs free energy tools were then coupled by randomly sampling the atmospheric state posterior distribution for relevant parameters and passing those randomized instances as inputs to the Gibbs free energy tool. Repeating this process thousands of times generates a posterior distribution for the available Gibbs free energy that is consistent with the simulated observation. The resulting posterior distribution allowed us to assess how observational uncertainty influences our ability to constrain and interpret chemical disequilibrium biosignatures.

The retrieval model

The rfast model³³ was adopted for the atmospheric retrievals. It incorporates a radiative transfer forward model, an instrument noise model and a retrieval tool to enable rapid investigations based on remote-sensing of exoplanet atmospheres. The radiative transfer forward model is capable of simulating (1) both one-dimensional and three-dimensional views of an exoplanet in reflected light, (2) emission spectra and (3) transit spectra. It takes as input the atmospheric chemical and thermal state (including profiles of cloud properties). The retrieval package also uses a Bayesian sampling package (emcee) to call the aforementioned radiative transfer model while mapping out the posterior distribution for the atmospheric parameters used to fit a noisy observation⁴⁷.

Our retrieval simulations are done in one dimension by using the diffuse radiative transfer treatment for modelling directly imaged views of the planet. They reproduce what one might expect for a quadrature (or gibbous) phase observation of an Earth-like exoplanet. The rfast model performs the retrieval inference assuming an isothermal atmosphere and constant volume mixing-ratio profiles for input chemical species. Clouds are taken to be an equal blend of liquid water and ice. Additionally, clouds in simulated observations are assumed to cover 50% of the disk and have a vertical extent described by the cloud top height and cloud pressure extent in Feng et al.¹⁷. Our noise estimates are constant with wavelength and set by the noise specified for the V band to remain consistent with decadal studies and previous exo-Earth retrieval analyses^{17,19,20}.

Gibbs free energy model

The thermodynamics Gibbs free energy model from Krissansen-Totton et al.^{11,12} was adopted to calculate chemical disequilibrium biosignatures. The Gibbs free energy is a thermodynamic state function that describes the maximum amount of work a chemical process can produce at constant pressure and temperature²²:

$$G = \sum_i^N \left(\frac{\partial G}{\partial n_i} \right) n_i, \quad (1)$$

where n_i is the moles of species i , $\partial G / \partial n_i$ is the change in Gibbs free energy with respect to the moles of a given species and the sum is over the total

number of species in the system (N). The overall Gibbs free energy of a given state can be rewritten in terms of thermodynamic activity and the standard Gibbs free energy of formation for a given species:

$$\Delta G_{(T,P)} = \sum_i^N \left(\Delta_f G_{i(T,P)}^\circ + RT \ln \left(\frac{P n_i}{n_T} \gamma_{fi} \right) \right) n_i, \quad (2)$$

where $\Delta_f G_{i(T,P)}^\circ$ is the Gibbs free energy of formation for a given species (determined at a given global mean surface temperature T and reference pressure P_r), n_T is the total number of moles and γ_{fi} is the activity coefficient. The utility of the Gibbs free energy is that it is minimized at thermodynamic equilibrium, which allows us to model the theoretical equilibrium state at a given temperature and pressure without explicitly considering individual chemical reactions.

Each observational scenario that was simulated considers the target as a closed, well-mixed system at constant global surface pressure and constant characteristic global temperature¹¹. The Gibbs free energy model first computes the Gibbs free energy of the system given an input atmospheric state (for example, usually an instance of gas mixing ratios, atmospheric temperature and surface pressure from the atmospheric retrieval model) and subsequently solves for the equilibrium species mixing ratios, such that the Gibbs free energy is minimized and atoms are conserved. An interior points method, implemented using Matlab's `fmincon` function, was used to minimize and solve for the equilibrium state. (Supplementary Fig. 4 details the initial and equilibrium abundances for all the species.) The difference between the Gibbs energy of the input atmospheric state and the equilibrium state quantifies the available Gibbs free energy:

$$\Phi \equiv G_{(T,P)}(n_{\text{initial}}) - G_{(T,P)}(n_{\text{eq}}). \quad (3)$$

The available Gibbs free energy (Φ) is, henceforth, used to quantify the chemical disequilibrium and is measured in joules of available free energy per mole of atmosphere^{11,12}, where n_{initial} and n_{eq} are the initial/observed and equilibrium mixing ratios, respectively. A large available Gibbs free energy indicates strong planetary chemical disequilibrium (for example, the modern Earth atmosphere and ocean system at 2,326 J mol⁻¹). Conversely, a low available Gibbs free energy indicates weak chemical disequilibrium. Most planetary bodies in our Solar System, like Jupiter, Venus and Uranus, all have well below 1 J mol⁻¹ of available free energy¹¹.

Thermodynamics calculations

Supplementary Fig. 4 shows an equilibrium calculation for the high Proterozoic abundance case presented in the main text. O₂, N₂, H₂O, CO₂, NH₃, CH₄, H₂, N₂O and O₃ are all included in the calculation. The total available Gibbs free energy for this scenario is 24.24 J mol⁻¹. The blue bars show the observed mixing ratios of each species, the red bars represent the equilibrium mixing ratios of each species and the yellow bars show the change in mixing ratio between the equilibrium and observed abundances. O₂ and CH₄ have notably large observed mixing ratios and also have large differences between their observed and equilibrium abundances. This indicates that these two species are the main drivers of chemical disequilibrium in the atmosphere. NH₃, H₂, N₂O and O₃ all contribute to the overall available free energy. However, their low relative abundances (in comparison to O₂ and CH₄) mean that the contribution of free energy from these species is negligible. Therefore, NH₃, H₂ and N₂O were excluded from the retrieval analysis and held at their equilibrium abundances when computing the available Gibbs free energy posterior distribution. O₃ was kept in the analysis as it is a photochemical byproduct of O₂ and, thus, useful to constrain alongside O₂.

Atmospheric modelling of the Proterozoic Earth

Self-consistent atmospheric models were generated using the photochemical model component of the Atmos tool^{48,49}. Atmos is a coupled

photochemical-climate model that uses planetary inputs (for example, chemical species mixing ratios, associated chemical reactions, gravity, surface pressure, surface temperature and stellar spectrum) to calculate the steady-state profiles of chemical species present in the atmosphere. In the overall analysis, the default solar spectrum was used to model Earth-like cases relevant to reflected-light observations³⁰. In the model, this solar spectrum was then adjusted with an input parameter (TIMEGA) to scale the solar flux to its appropriate insolation 1.3 Gyr ago. The TRAPPIST-1 spectrum⁵¹ was used for the TRAPPIST-1 simulations mentioned in the text. All the atmospheric cases modelled in this study assumed a total fixed surface pressure of 1 bar. A suite of cases spanning from low to high concentrations of O₂, CH₄ and CO₂ (input values outlined in Table 1) were explored to capture broad uncertainty in the abundance of certain atmospheric species during the Proterozoic eon and referenced to the 'model low' and 'model high' values from Table 1 in Robinson and Reinhard²¹. The medium-abundance case was computed by taking the logarithmic geometric average of the high and low values. These generated profiles were used to produce realistic atmospheric spectra with the `rfast` forward model that were then retrieved on. Note that the changes in CO₂ abundance did not have a substantial impact on the uncertainty of the available Gibbs free energy.

Simulated rfast observations

Reflected-light observations in this study were modelled after direct-imaging Decadal Survey mission concepts with ultraviolet (0.2–0.4 μm), optical (0.4–1.0 μm) and near-infrared (1.0–1.8 μm) band-passes at resolving powers of 7, 140 and 70, respectively^{19,20}. Each instance of a simulated noisy spectrum was produced with randomized error bars and with the prescribed SNR taken to apply at 0.55 μm (consistent with earlier exo-Earth studies).

Reflected-light retrievals

Outlined in Supplementary Fig. 3 are the marginal posterior distributions for the mixing ratios of H₂O (Supplementary Fig. 3a), CO₂ (Supplementary Fig. 3b) and O₃ (Supplementary Fig. 3c), along with the retrieved atmospheric pressure (Supplementary Fig. 3d) for the high (green), medium (purple) and low (blue) abundance scenarios. These retrieved parameters were included in the random sampling used to compute the available Gibbs free energy posteriors (Fig. 1) but did not have a substantial influence on the uncertainty. However, constraining parameters like H₂O, CO₂ and surface pressure are essential for inferring the climate and habitability of exoplanets. Additionally, O₃ can be used as a proxy for loosely approximating the O₂ abundance for less oxygenated atmospheres since O₃ can remain detectable even at low O₂ concentrations^{5,6,52}. The caveat is that other factors (for example, the stellar host type and stellar ultraviolet flux) must be well characterized³¹. A comprehensive list of the planetary parameters included in the retrieval analysis are shown in Supplementary Table 1.

Transit retrievals and available Gibbs free energy inference

The successful launch of the JWST and the prospects for characterizing Earth-like planets in the habitable zone of M dwarf stars motivated attempts to constrain the available Gibbs free energy of a Proterozoic Earth-like planet orbiting the M dwarf TRAPPIST-1. For all three atmospheric cases and simulated observations with the NIRSpec instrument, our results (Supplementary Figs. 1 and 2) indicate that it is extremely challenging, requiring less than 5 ppm noise.

In Supplementary Fig. 1, the marginal posterior distributions for the O₂ abundance (Supplementary Fig. 1a), CH₄ abundance (Supplementary Fig. 1b) and atmospheric temperature (Supplementary Fig. 1c) are outlined at the high-, medium- and low-abundance cases for a Proterozoic Earth-like planet orbiting an M dwarf and inferred from simulated transit observations with the JWST NIRSpec instrument. For O₂, in particular, these results show that it is very difficult to constrain the atmospheric

abundance of O₂ at each of the observational noise levels (5 and 10 ppm), either of which would be challenging for JWST to achieve for current best-case targets. This outcome was to be expected given that detecting biogenic O₂ abundances with JWST is a known challenge^{29,30,53,54}. The lack of constraints on the O₂ abundance also make inferring the chemical disequilibrium energy of a Proterozoic Earth-like exoplanet orbiting a late-type star too challenging for JWST. In Supplementary Fig. 2, the available Gibbs free energy posteriors inferred from these observations are shown for the high (Supplementary Fig. 2a), medium (Supplementary Fig. 2b) and low (Supplementary Fig. 2c) abundance cases. The posterior distributions for all abundance cases and noise levels demonstrate that a noise floor of <5 ppm would be required to obtain tight constraints on the available Gibbs free energy for these Proterozoic Earth-like scenarios. This <5 ppm noise estimate is smaller than some predicted estimates (of the order of tens of parts per million) for the noise floor^{2,55}. It is, therefore, unlikely that JWST could constrain the available Gibbs free energy for a Proterozoic Earth-like planet.

Data availability

All the source data that corresponds to the results of this work (for example, spectral data, available Gibbs free energy distributions and retrieval parameter distributions) have been published on Zenodo⁵⁶ and are available to download from <https://zenodo.org/record/8335447>. The initial release of the rfast spectral retrieval model can be accessed from <https://zenodo.org/record/7327817>. The Atmos model is publicly available and can be accessed at <https://github.com/VirtualPlanetaryLaboratory/atmos>. The Matlab version of the thermodynamics model from Krissansen-Totton et al.^{11,12} is available from co-author J.K.T.'s personal website: <http://www.kriststott.com/code.html>. Source data are provided with this paper.

Code availability

The code is available as follows: rfast <https://zenodo.org/record/7327817>; Atmos <https://github.com/VirtualPlanetaryLaboratory/atmos>; and the thermodynamics model <http://www.kriststott.com/code.html>.

References

- Gardner, J. P. et al. The James Webb Space Telescope. *Space Sci. Rev.* **123**, 485–606 (2006).
- Greene, T. P. et al. Characterizing transiting exoplanet atmospheres with JWST. *Astrophys. J.* **817**, 17 (2016).
- Ahrer, E.-M. et al. Identification of carbon dioxide in an exoplanet atmosphere. *Nature* **614**, 649–652 (2023).
- National Academies of Sciences, Engineering, and Medicine. *Pathways to Discovery in Astronomy and Astrophysics for the 2020s* (National Academies Press, 2021).
- Schwieterman, E. W. et al. Exoplanet biosignatures: a review of remotely detectable signs of life. *Astrobiology* **18**, 663–708 (2018).
- Meadows, V. S. et al. Exoplanet biosignatures: understanding oxygen as a biosignature in the context of its environment. *Astrobiology* **18**, 630–662 (2018).
- Madhusudhan, N. Exoplanetary atmospheres: key insights, challenges, and prospects. *Annu. Rev. Astron. Astrophys.* **57**, 617–663 (2019).
- Lovelock, J. E. A physical basis for life detection experiments. *Nature* **207**, 568–570 (1965).
- Hitchcock, D. R. & Lovelock, J. E. Life detection by atmospheric analysis. *Icarus* **7**, 149–159 (1967).
- Lovelock, J. E. & Kaplan, I. R. Thermodynamics and the recognition of alien biospheres [and Discussion]. *Proc. R. Soc. Lond. B* <https://doi.org/10.1098/rspb.1975.0051> (1975).
- Krissansen-Totton, J., Bergsman, D. S. & Catling, D. C. On detecting biospheres from chemical thermodynamic disequilibrium in planetary atmospheres. *Astrobiology* **16**, 39–67 (2016).
- Krissansen-Totton, J., Olson, S. & Catling, D. C. Disequilibrium biosignatures over Earth history and implications for detecting exoplanet life. *Sci. Adv.* **4**, ea05747 (2018).
- Wogan, N. F. & Catling, D. C. When is chemical disequilibrium in Earth-like planetary atmospheres a biosignature versus an anti-biosignature? Disequilibrium from dead to living worlds. *Astrophys. J.* **892**, 127 (2020).
- Madhusudhan, N. & Seager, S. A temperature and abundance retrieval method for exoplanet atmospheres. *Astrophys. J.* **707**, 24 (2009).
- Benneke, B. & Seager, S. Atmospheric retrieval for super-Earths: uniquely constraining the atmospheric composition with transmission spectroscopy. *Astrophys. J.* **753**, 100 (2012).
- Line, M. R. et al. A systematic retrieval analysis of secondary eclipse spectra. I. A comparison of atmospheric retrieval techniques. *Astrophys. J.* **775**, 137 (2013).
- Feng, Y. K. et al. Characterizing Earth analogs in reflected light: atmospheric retrieval studies for future space telescopes. *Astron. J.* **155**, 200 (2018).
- Barstow, J. K. et al. A comparison of exoplanet spectroscopic retrieval tools. *Mon. Not. R. Astron. Soc.* **493**, 4884–4909 (2020).
- Gaudi, B. S., Seager, S., Mennesson, B., Kiessling, A. & Warfield, K. R. The Habitable Exoplanet Observatory. *Nat. Astron.* **2**, 600–604 (2018).
- Roberge, A. & Moustakas, L. A. The Large Ultraviolet/Optical/Infrared Surveyor. *Nat. Astron.* **2**, 605–607 (2018).
- Robinson, T. & Reinhard, C. in *Planetary Astrobiology* (eds Meadows, V., Arney, G., Schmidt, B. & Marais, D. J. D.) (Univ. Arizona Press, 2020).
- Engel, T. & Reid, P. *Thermodynamics, Statistical Thermodynamics, and Kinetics* (Pearson Education, 2019).
- Robinson, T. D., Stapelfeldt, K. R. & Marley, M. S. Characterizing rocky and gaseous exoplanets with 2 m class space-based coronagraphs. *Publ. Astron. Soc. Pac.* **128**, 025003 (2016).
- Mamajek, E. & Stapelfeldt, K. NASA ExEP Mission star list for the Habitable Worlds Observatory: most accessible targets to survey for potentially habitable exoplanets, (NASA ExEP, 2023); exoplanetarchive.ipac.caltech.edu/docs/2645_NASA_ExEP_Target_List_HWO_Documentation_2023.pdf
- Kawahara, H. et al. Can ground-based telescopes detect the oxygen 1.27 μm absorption feature as a biomarker in exoplanets? *Astrophys. J.* **758**, 13 (2012).
- Rodler, F. & López-Morales, M. Feasibility studies for the detection of O₂ in an Earth-like exoplanet. *Astrophys. J.* **781**, 54 (2014).
- Hardegree-Ullman, K. K., Apai, D., Bergsten, G. J., Pascucci, I. & López-Morales, M. Bioverse: a comprehensive assessment of the capabilities of extremely large telescopes to probe Earth-like O₂ levels in nearby transiting habitable-zone exoplanets. *Astron. J.* **165**, 267 (2023).
- Currie, M. H., Meadows, V. S. & Rasmussen, K. C. There's more to life than O₂: simulating the detectability of a range of molecules for ground-based, high-resolution spectroscopy of transiting terrestrial exoplanets. *Planet. Sci. J.* **4**, 83 (2023).
- Wunderlich, F. et al. Detectability of atmospheric features of Earth-like planets in the habitable zone around M dwarfs. *Astron. Astrophys.* **624**, A49 (2019).
- Faucher, T. J. et al. Sensitive probing of exoplanetary oxygen via mid-infrared collisional absorption. *Nat. Astron.* **4**, 372–376 (2020).
- Kozakis, T., Mendonça, J. M. & Buchhave, L. A. Is ozone a reliable proxy for molecular oxygen? I. The O₂–O₃ relationship for Earth-like atmospheres. *Astron. Astrophys.* **665**, A156 (2022).
- Konrad, B. S. et al. Large Interferometer For Exoplanets (LIFE). III. Spectral resolution, wavelength range, and sensitivity requirements based on atmospheric retrieval analyses of an exo-Earth. *Astron. Astrophys.* **664**, A23 (2022).

33. Robinson, T. D. & Salvador, A. Exploring and validating exoplanet atmospheric retrievals with Solar System analog observations. *Planet. Sci. J.* **4**, 10 (2023).
34. Gialluca, M. T., Robinson, T. D., Rugheimer, S. & Wunderlich, F. Characterizing atmospheres of transiting Earth-like exoplanets orbiting M dwarfs with James Webb Space Telescope. *Publ. Astron. Soc. Pac.* **133**, 054401 (2021).
35. Quanz, S. P. et al. Large Interferometer For Exoplanets (LIFE). I. Improved exoplanet detection yield estimates for a large mid-infrared space-interferometer mission. *Astron. Astrophys.* **664**, A21 (2022).
36. Segura, A. et al. Biosignatures from Earth-like planets around M dwarfs. *Astrobiology* **5**, 706–725 (2005).
37. Arney, G. N. The K dwarf advantage for biosignatures on directly imaged exoplanets. *Astrophys. J. Lett.* **873**, L7 (2019).
38. Cowan, N. B. et al. Alien maps of an ocean-bearing world. *Astrophys. J.* **700**, 915 (2009).
39. Robinson, T. D., Meadows, V. S. & Crisp, D. Detecting oceans on extrasolar planets using the glint effect. *Astrophys. J. Lett.* **721**, L67 (2010).
40. Zuger, M. E., Kasting, J. F., Williams, D. M., Kane, T. J. & Philbrick, C. R. Light scattering from exoplanet oceans and atmospheres. *Astrophys. J.* **723**, 1168 (2010).
41. Lustig-Yaeger, J. et al. Detecting ocean glint on exoplanets using multiphase mapping. *Astron. J.* **156**, 301 (2018).
42. Harman, C. E. et al. Abiotic O₂ levels on planets around F, G, K, and M stars: effects of lightning-produced catalysts in eliminating oxygen false positives. *Astrophys. J.* **866**, 56 (2018).
43. Luger, R. & Barnes, R. Extreme water loss and abiotic O₂ buildup on planets throughout the habitable zones of M dwarfs. *Astrobiology* **15**, 119–143 (2015).
44. Domagal-Goldman, S. D., Segura, A., Claire, M. W., Robinson, T. D. & Meadows, V. S. Abiotic ozone and oxygen in atmospheres similar to prebiotic Earth. *Astrophys. J.* **792**, 90 (2014).
45. Wordsworth, R. & Pierrehumbert, R. Abiotic oxygen-dominated atmospheres on terrestrial habitable zone planets. *Astrophys. J. Lett.* **785**, L20 (2014).
46. Krissansen-Totton, J., Fortney, J. J., Nimmo, F. & Wogan, N. Oxygen false positives on habitable zone planets around Sun-like stars. *AGU Adv.* **2**, e2020AV000294 (2021).
47. Foreman-Mackey, D., Hogg, D. W., Lang, D. & Goodman, J. emcee: the MCMC hammer. *Publ. Astron. Soc. Pac.* **125**, 306 (2013).
48. Arney, G. et al. The pale orange dot: the spectrum and habitability of hazy Archean Earth. *Astrobiology* **16**, 873–899 (2016).
49. Arney, G. N. et al. Pale orange dots: the impact of organic haze on the habitability and detectability of Earthlike exoplanets. *Astrophys. J.* **836**, 49 (2017).
50. Thuillier, G. et al. Solar irradiance reference spectra for two solar active levels. *Adv. Space Res.* **34**, 256–261 (2004).
51. Peacock, S., Barman, T., Shkolnik, E. L., Hauschildt, P. H. & Baron, E. Predicting the extreme ultraviolet radiation environment of exoplanets around low-mass stars: The TRAPPIST-1 system. *Astrophys. J.* **871**, 235 (2019).
52. Meadows, V. S. Reflections on O₂ as a biosignature in exoplanetary atmospheres. *Astrobiology* **17**, 1022–1052 (2017).
53. Krissansen-Totton, J., Garland, R., Irwin, P. & Catling, D. C. Detectability of biosignatures in anoxic atmospheres with the James Webb Space Telescope: a TRAPPIST-1e case study. *Astron. J.* **156**, 114 (2018).
54. Lustig-Yaeger, J., Meadows, V. S. & Lincowski, A. P. The detectability and characterization of the TRAPPIST-1 exoplanet atmospheres with JWST. *Astron. J.* **158**, 27 (2019).
55. Rustamkulov, Z., Sing, D. K., Liu, R. & Wang, A. Analysis of a JWST NIRSpec lab time series: characterizing systematics, recovering exoplanet transit spectroscopy, and constraining a noise floor. *Astrophys. J. Lett.* **928**, L7 (2022).
56. Young, A. V. Source data for manuscript ‘Inferring Chemical Disequilibrium Biosignatures for Proterozoic Earth-like Exoplanets’. *Zenodo* <https://doi.org/10.5281/zenodo.8335447> (2023).

Acknowledgements

We would all like to acknowledge support from the NASA Exobiology Program and NASA's Nexus for Exoplanet System Science Virtual Planetary Laboratory. We would also like to acknowledge support from NASA's Exoplanets Research Program, the Habitable Worlds Program and the NASA Interdisciplinary Consortia for Astrobiology Research Program through the Alternative Earths team. We acknowledge support from the Cottrell Scholar Program administered by the Research Corporation for Science Advancement. Finally, we acknowledge support from the Sellers Exoplanet Environments Collaboration at the Goddard Space Flight Center and ROCKE-3D: The evolution of Solar System worlds through time, both of which are funded by the NASA Planetary Science Divisions Internal Scientist Funding Model. This research was supported by Grant Nos. 80NSSC18K0349 (A.V.Y., T.D.R., J.K.T., E.W.S., M.J.W., L.E.S., G.N.A., C.T.R., M.R.L., D.C.C. and J.D.W.), 80NSSC18K0829 (A.V.Y., T.D.R., E.W.S., D.C.C. and N.F.W.), 80NSSC18K0349, 80NSSC20K0226 (T.D.R.) and 80NSSC21K059 (E.W.S. and C.T.R.).

Author contributions

A.V.Y. conducted all the atmospheric retrievals outlined in this work, developed the code to couple the retrieval results to the Gibbs free energy model, and computed the available Gibbs free energy posteriors for all the simulated cases. T.D.R. adapted the code and developed rfast in correspondence with the retrieval analyses performed in this work and is the principal investigator of the project. J.K.T. distributed the most up-to-date version of the thermodynamics model used in this work and contributed to the necessary code development and adaptation for the thermodynamic simulations. E.W.S. provided the Atoms-generated atmospheric compositions for each of the abundance scenarios outlined in this work. All authors contributed to both project development and the writing or editing of the paper and approved the scientific content.

Competing interests

The authors declare no competing interests.

Additional information

Supplementary information The online version contains supplementary material available at <https://doi.org/10.1038/s41550-023-02145-z>.

Correspondence and requests for materials should be addressed to Amber V. Young.

Peer review information *Nature Astronomy* thanks the anonymous reviewers for their contribution to the peer review of this work.

Reprints and permissions information is available at www.nature.com/reprints.

Publisher's note Springer Nature remains neutral with regard to jurisdictional claims in published maps and institutional affiliations.

Open Access This article is licensed under a Creative Commons Attribution 4.0 International License, which permits use, sharing, adaptation, distribution and reproduction in any medium or format, as long as you give appropriate credit to the original author(s) and the source, provide a link to the Creative Commons license, and indicate if changes were made. The images or other third party material in this article are included in the article's Creative Commons license, unless indicated otherwise in a credit

line to the material. If material is not included in the article's Creative Commons license and your intended use is not permitted by statutory regulation or exceeds the permitted use, you will need to obtain permission directly from the copyright holder. To view a copy of this license, visit <http://creativecommons.org/licenses/by/4.0/>.

© The Author(s) 2024